Nonlinear hydrodynamic characteristics of multi-body platform system

Xiudi Ren[1], Longbin Tao[1]*

[1] Department of Naval Architecture, Ocean & Marine Engineering, University of Strathclyde, Glasgow, G4 0LZ, UK.

Abstract

Along with the technology development of ocean resources, offshore platforms are gradually becoming larger and more complex. Recent development of the oil and gas field in the deep-water region often involves multiple floating platforms adjacent to each other to perform more complex functions for oil and gas production. This paper describes the investigation carried out on the dynamic responses of a two platforms system containing a Tension Leg Platform (TLP) and a tender assisted drilling (TAD) with a flexible connection between the two platforms. The mooring lines and tendons are taken into consideration in the coupled analysis of the multi-body platform's system. The motion responses and wave load characteristics on the two platforms in multi-body coupled model are investigated in the numerical simulation. Compared to the situation of the two platforms in isolation, it is revealed that the motion responses for the two platforms in coupled model are altered by the combined effects of the platforms' interaction and constrain by the connection. The interaction between platforms can increase both the first- and second-order wave force on platforms in the arrangement direction of two platforms. Quantitative analysis demonstrates their relative importance and thus provides much-needed guidance in practical design of the coupled system.

1. Introduction

[1] Xiudi Ren, PhD student, Department of Naval Architecture, Ocean & Marine Engineering, University of Strathclyde, Glasgow, G4 0LZ, UK. Email: xiudi.ren@strath.ac.uk

[1] Longbin Tao, Professor, Department of Naval Architecture, Ocean & Marine Engineering, University of Strathclyde, Glasgow, G4 0LZ, UK. Email: longbin.tao@strath.ac.uk (* corresponding author)

Since the offshore oil and gas fields progressively moving towards deep-water, more complex functional requirements are desired for the oil and gas drilling and production platform system. The traditional individual offshore platform is replaced by the complex drilling and production system gradually. The platforms for producing and drilling or accommodating are always combined as a multi-body platform system (MPS) to achieve more functions and support [1, 2].

The Odin field is the first field development applying the concept of the combination of the different platforms. The project is consisting of a fixed jacked platform and a tender vessel [3]. With the first successful attempt, more tender support vessels are used with the nearshore fixed platforms. To explore the resource in deep-water, floating platforms are needed. Tension leg platform (TLP) is a widely employed option for oil and gas production in deep-water for its good stability at sea. Besides, the tender assisted drilling (TAD) system has a great economic benefit since it can provide several kinds of supports to the main production platform. The combination of TLP-TAD coupled system is often adopted during the drilling stage since the advantages of TLP's motion characteristics and TAD's outstanding supportive abilities [4].

As one of the critical aspects, the response of the mooring lines system and the bridge between two platforms are determined by the hydrodynamic characteristics of the multi-body system. The accurate prediction of the multi-body hydrodynamic response is very important for the coupled analysis between the bodies and mooring lines system. The interaction between multi-body and the wave which contains diffraction and radiation makes the solution of the wave load and prediction of the motion response more difficult. Additionally, the nonlinear mooring system and the bridge between two platforms make the coupled analysis of multi-body more complex to solve. There are some investigations carried out on the hydrodynamic characteristics of multi-body system which contains two large floating offshore structures. Among some of the pioneers, Kim [5] applied the 2D strip method in the 1970s solving the interaction between slender structures in waves. Loken [6] calculated the motion response and the wave drift force for a multi-body system based on the potential theory. Comparing with the model test values, the result of drift force is lower since the neglection of the viscosity. The nonlinear wave run up and air-gap response in multiple columns Semi-submersible were conducted by Lu et al. [7].

The multi-body system is also widely applied in the drilling and production of oil and gas and storage and loading platforms like FPSO and FLNG with side-by-side arrangement [8, 9]. Hydrodynamic characteristics of two ships coupled motion response, wave load and some issues like water surface resonance in the narrow gap between ships are investigated [10-12]. More recently, Ganesan and Sen [13] conducted a numerical simulation of an FPSO with a shuttle side-by-side in 3D numerical wave tank. Gap resonance was studied by implementing a damping lid method with a constant damping factor to solve the overestimation of free surface. Zhao et al. [14] studied the gap resonance between two barges investigating the group dynamics and wave propagation of the resonant responses in a narrow gap by model test. It showed that the gap resonance is sensitive to the approaching wave heading direction and the group velocity of the resonant modes is smaller than that for deep water free waves. Huang et al. [15] carried out both experiment and numerical study to investigate the response of the gangway between two side-by-side FPSOs. It is noted that some researchers also applied the viscous fluid based on CFD to solve such kind of hydrodynamic issues. Ok et al. [16] solved the motion of side-by-side floating vessels by using the finite-volume method to solve the N-S equation with OpenFOAM. Although CFD method can correctly solve multi-body hydrodynamic problems, it is very time-consuming compared to potential theory which is widely used at present.

To date, most studies on the topic have focused on the hydrodynamic characteristics between ships or jacked platforms [17, 18]. There are also some studies on the hydrodynamic interaction between two floating platforms in a multi-body platform system. Xia and Taghipour [19] conducted an eigenvalue study of Tension Leg Platform (TLP) with a tender assisted drilling (TAD) in longitudinal motion of the two bodies in the multi-body system. Choi et al. [20] conducted an experimental study on TLP and Semi-sub's motion response characteristics. It is observed that the coupled low-frequency motion periods of the TLP-tender semi-submersible platform are generally shorter than those of individual structure due to additional hawser and moorings between the two floating bodies. Sun et al. [21] investigated the interaction effects between large-volume substructures and floating barge. Ramirez and Fernandes [22] analysed the hydrodynamic characteristics of TLP-TAD system using finite element method (FEM). However, the work is mainly on the first-order. Liang and Tao [23] calculated the two semi-submersible platform system under the current condition to examine the collision condition. Abyn et al. [24] focused on the motion effect caused by TLP on the TAD system with a towing tank model test and concluded that the radiation wave caused by TLP would increase the TAD's surge and heave motion amplitude. Maimun, et al. [25] investigated the hydrodynamic interactions of two floating platforms in close proximity to find out the relative motion in surge direction. There are also some studies reported in the literature specifically focused on the dynamics of the hawsers and gangways connecting the two platforms. Dong et al [26] investigated the motion of gangway between two platforms in the multi-body platform system using both model test and numerical simulation. The results of gangway extension and rotation show that the dominant degree-of-freedom (DOF) of global motion for gangway responses is identical under different headings. The extreme value predictions of gangway responses are also performed based on Weibull distribution in their research.

As one of the distinct features, nonlinear hydrodynamic characteristics of floating bodies in the multi-body system are essential for the design and safe operation of the mooring lines and gangway between platforms in harsh offshore environment. To obtain the nonlinear motion response and wave force on the structures consisting multi-body platform system, coupled nonlinear analysis is conducted in this study. Based on the detailed contributions of the linear and nonlinear wave forces explicitly calculated, a quantitative examination has been made by comparing the results of the individual platform and the coupled multi-body platform cases. The present numerical model is validated against the data from the model tests carried out by Dong et al. [26]. The main results of motion responses and wave loads for the individual platform and multi-body platform are compared in Section 4.1 and Section 4.2. Nonlinear effects and their contributions towards the wave force and motion responses in the multi-body platform system are examined in detail. The wave forces on bodies in coupled model and isolation model in time domain are calculated in Section 4.3. The main conclusions are summarized in Section 5.

2. Theoretical background

2.1 Multi-body hydrodynamic

The fluid is assumed inviscid, irrotational and incompressible. The nonlinear solutions for surface elevation and wave load are obtained by applying the potential theory up to the second-order in diffraction/radiation analysis. The incident wave is assumed to be small amplitude and perturbation is applicable [27, 28].

$$\phi = \varepsilon\phi^{(1)} + \varepsilon^2\phi^{(2)} + \ldots \quad (1)$$

$$\phi^{(1)}\left(x,y,z,t\right) = \mathrm{Re}\left\{\phi^{(1)}(x,y,z)e^{-i\omega t}\right\} \quad (2)$$

$$\phi^{(2)}(x,y,z,t) = \mathrm{Re}\left\{\phi^{(2)}(x,y,z)e^{-i2\omega t}\right\} + \overline{\phi}^{(2)}(x,y,z) \quad (3)$$

where ϕ is the total velocity potential, $\phi^{(1)}(x,y,z,t)$is the first-order velocity potential and $\phi^{(2)}(x,y,z,t)$ is the second-order velocity potential. $\phi^{(1)}(x,y,z)$ and $\phi^{(2)}(x,y,z)$ are the time-independent velocity potentials and $\bar{\phi}^{(2)}$ is the steady term of the velocity potential. The first-order and the second-order velocity potential satisfies Laplace's equation and the boundary conditions in diffraction analysis. For the first-order,

$$\nabla^2\phi_D^{(1)} = 0 \qquad z > 0 \quad (4a)$$

$$(-\omega^2 + g\frac{\partial}{\partial z})\phi_D^{(1)} = 0 \qquad z = 0\left(S_F\right) \quad (4b)$$

$$\frac{\partial\phi_D^{(1)}}{\partial z} = 0 \qquad z = -h \quad (4c)$$

$$\frac{\partial\phi_D^{(1)}}{\partial n} = -\frac{\partial\phi_I^{(1)}}{\partial n} \qquad \text{at structural boundary } S_b \quad (4d)$$

$$\lim_{k\rho\to\infty}\rho^{1/2}(\frac{\partial}{\partial\rho} - ik)\phi_D^{(1)} = 0 \quad (4e)$$

and for the second-order diffraction analysis,

$$\nabla^2\phi_D^{(2)} = 0 \qquad z > 0 \quad (5a)$$

$$(-4\omega^2 + g\frac{\partial}{\partial z})\phi_D^{(2)} = q \qquad z = 0\left(S_F\right) \quad (5b)$$

$$\frac{\partial\phi_D^{(2)}}{\partial z} = 0 \qquad z = -h \quad (5c)$$

$$\frac{\partial\phi_D^{(2)}}{\partial n} = -\frac{\partial\phi_I^{(2)}}{\partial n} \qquad \text{at structural boundary } S_b \quad (5d)$$

$$\lim_{k\rho\to\infty}\rho^{1/2}(\frac{\partial}{\partial\rho} - ik)\phi_D^{(2)} = 0 \quad (5e)$$

where ϕ_D is the diffracted wave potential, ω is the incident wave frequency, and *k* is the incident wave number. The right-hand side term "*q*" in (5b) is the non-homogeneous term which represents the free surface condition and shows the quadratic production of the first-order potential. The first-order and second-order boundary value problems (BVPs) are solved by direct boundary element method. Full quadratic transfer functions (QTFs) for both sum-frequency and difference-frequency load are derived according to Kim and Yue [28].

2.2 Wave load

In order to examine the detailed contributions and the nonlinearity, three parts of the wave forces are calculated separately [29],

$$F_j = F_j^{(1)} + F_j^{(2)} + \overline{F}_j^{(2)} \tag{6}$$

where the first-order force is

$$F_j^{(1)} = -\rho \iint_{S_b^{(0)}} \frac{\partial \phi^{(1)}}{\partial t} n_j ds \quad (j = 1, 2, \ldots, 6) \tag{7}$$

The second-order force can be decomposed into three components,

$$F_j^{(2)} = F_j^{(21)} + F_j^{(22)} - \overline{F}_j^{(2)} \quad (j = 1, 2, \cdots, 6) \tag{8}$$

where

$$F_j^{(21)} = -\frac{1}{2}\rho \iint_{S_b^{(0)}} \left|\nabla \phi^{(1)}\right|^2 n_j ds + \frac{1}{2}\rho g \int_l (\eta^{(1)})^2 n_j dl \quad (j = 1, 2, \cdots, 6) \tag{9}$$

$$F_j^{(22)} = -\rho \iint_{S_b^{(0)}} \frac{\partial \phi^{(2)}}{\partial t} n_j ds \quad (j = 1, 2, \cdots, 6) \tag{10}$$

$$\overline{F}_j^{(2)} = -\frac{1}{2}\rho \overline{\iint_{S_b^{(0)}} \left|\nabla \phi^{(1)}\right|^2 n_j ds} + \frac{1}{2}\rho g \overline{\int_l (\eta^{(1)})^2 n_j dl} \quad (j = 1, 2, \cdots, 6) \tag{11}$$

$F_j^{(21)}$ is the wave force due to the first-order velocity potential and surface elevation, and $F_j^{(22)}$ is dependent on the second-order velocity potential and $\overline{F}_j^{(2)}$ is the steady term TLP is very sensitive to the high-frequency wave load especially on the vertical plan motions, and the wave drift load will lead the drift motion of TAD which is the semi-submersible in the present study. It is essential to calculate the wave load on the TLP and TAD accurately for the reliable prediction of the performance of the multi-body platform system [30, 31].

To carry out the fully coupled motion analysis for the two floating platforms with mooring lines and hawsers, the motion equation is [32]:

$$\sum_{j=1}^{12} [-\omega^2 \left(M_{ij} + A_{ij}(\omega)\right) - i\omega B_{ij}(\omega) + C_{ij}]\xi_j(\omega) = F_i(\omega), \; i,j = 1, \ldots \ldots, 12 \tag{13}$$

in which, M_{ij} is the inertia matrix, C_{ij} is the hydrostatic restoring matrix. The hydrodynamic coefficients of the added mess, damping matrix and wave load are calculated by the potential flow software HydroD. The $i,j = 1,\ldots\ldots,6$ represent the hydrodynamic coefficients for body 1, and $i,j = 7,\ldots\ldots,12$ is for body 2 and the rest of the term are for the hydrodynamic interaction between TLP and TAD. The coupled time-domain analysis of the multi-body platform is operated by 3D coupled analysis software SIMA [33].

3. Description of coupled TLP and TAD configuration

The specifications of TLP and TAD investigated in the present study are given in Table 1. TLP is composed of four circular columns and rectangular pontoons. 8 tendons are attached to the columns (2 of each column) of the TLP. 4 steel catenary risers (SCRs) are connected to the pontoon for production as shown in Fig1. 2 back lines applied to the TLP are to restrict its movement towards TAD. TAD is designed based on a semi-submersible with 8 mooring lines (Fig 1). Details of the truncation method using in the experiment can be referred to [34, 35].

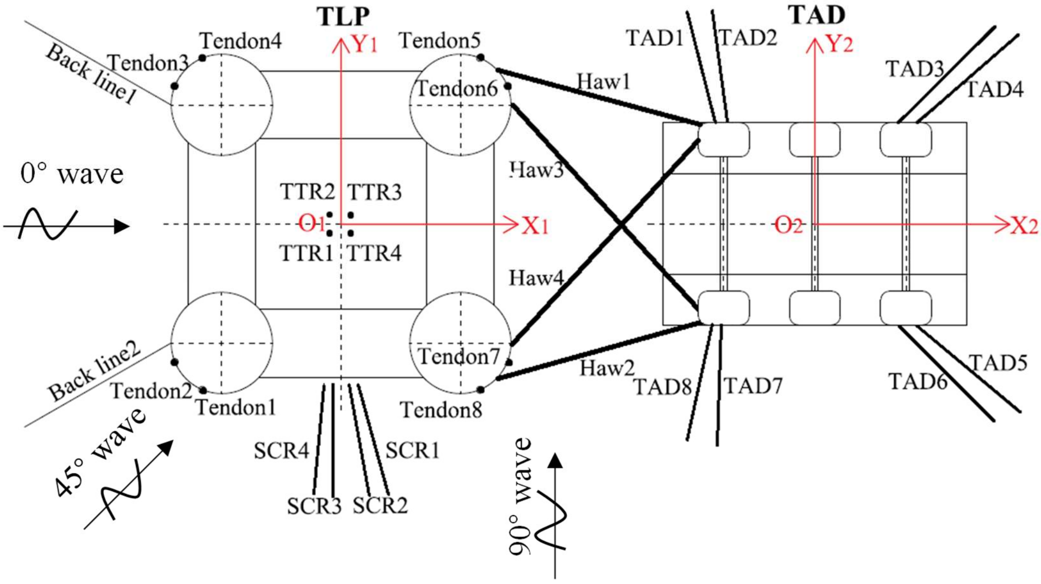

Fig 1 The arrangement of TLP and TAD in multi-body coupled model [26]

Table 1 Main particulars of TLP and TAD (full scale)

Parameter	Unit	TLP	TAD
Displacement	MT	5.09E4	1.73E4
Draft	m	22.2	9.75
XG	m	0.0	-0.1

KG	m	32	16.6
Roll gyradius	m	31.5	19.5
Pitch gyradius	m	30.2	31.2
Yaw gyradius	m	28.9	30.2

Since the symmetry of the platform of TLP and TAD, 0° and 45° wave headings are investigated for isolated TLP, isolated TAD and TLP-TAD coupled model. The experiment conducted by Dong et al. [26] in the Deepwater Offshore Basin at Shanghai Jiao Tong University is used as a primary benchmark for the extensive validation of the present numerical model.

Table 2 lists the random wave conditions for the present numerical study. JONSWAP wave spectrum with significant wave height H_s, peak wave period T_s and spectral steepness γ are selected. According to Dong et al. [26], the wind and current force were considered and replaced by the equivalent constant forces on platforms which are also applied in the present numerical simulation to replace the wind and current force. The viscous effect on the model is estimated by Morison equation and added to the damping matrix in the motion equations.

Table 2 Environment condition

Condition	Direction	H_s	T_P	γ
EC1	0	2.4	7	1.2
EC2	90	1.1	7	1.2

4. Results and discussion

4.1 Mesh convergence and Validation

Mesh sensitive study is conducted prior to the comprehensive numerical simulations of the multi-body platforms. The wave forces acting on both TLP and TAD are used to measure convergence of the numerical calculation. The meshes on the structure boundary and free water surface are investigated in the mesh convergence study for both the first-order and the second-order wave force calculated in the present study. The wave condition used in the mesh convergence study is from 0° whose frequency is 1.2rad/s.

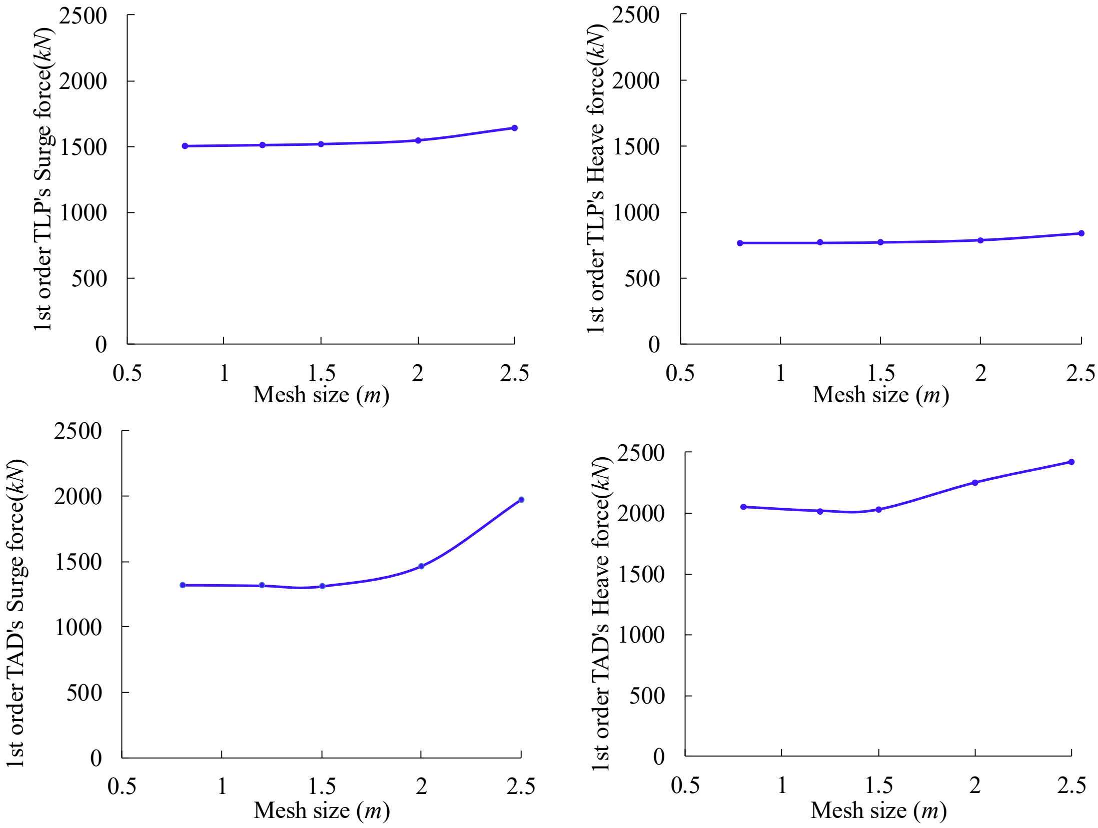

Fig 2 First-order surge and heave forces on TLP and TAD in coupled model using different meshes under 0° incident wave with frequency 1.2rad/s.

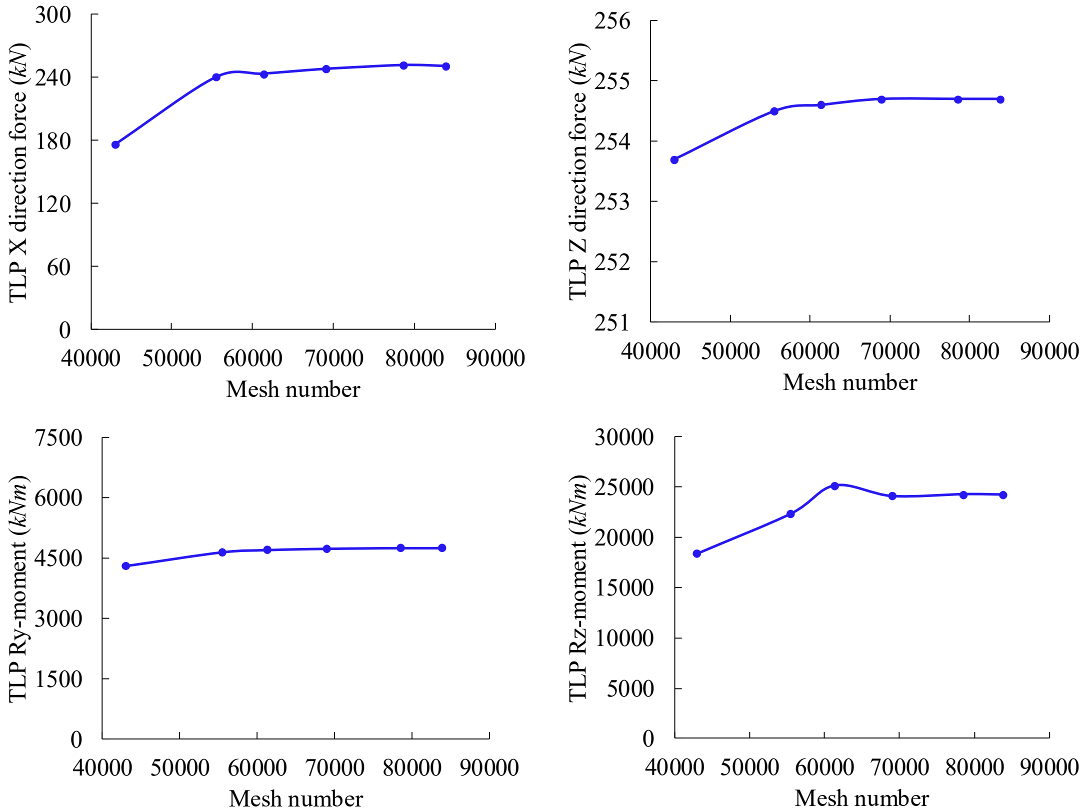

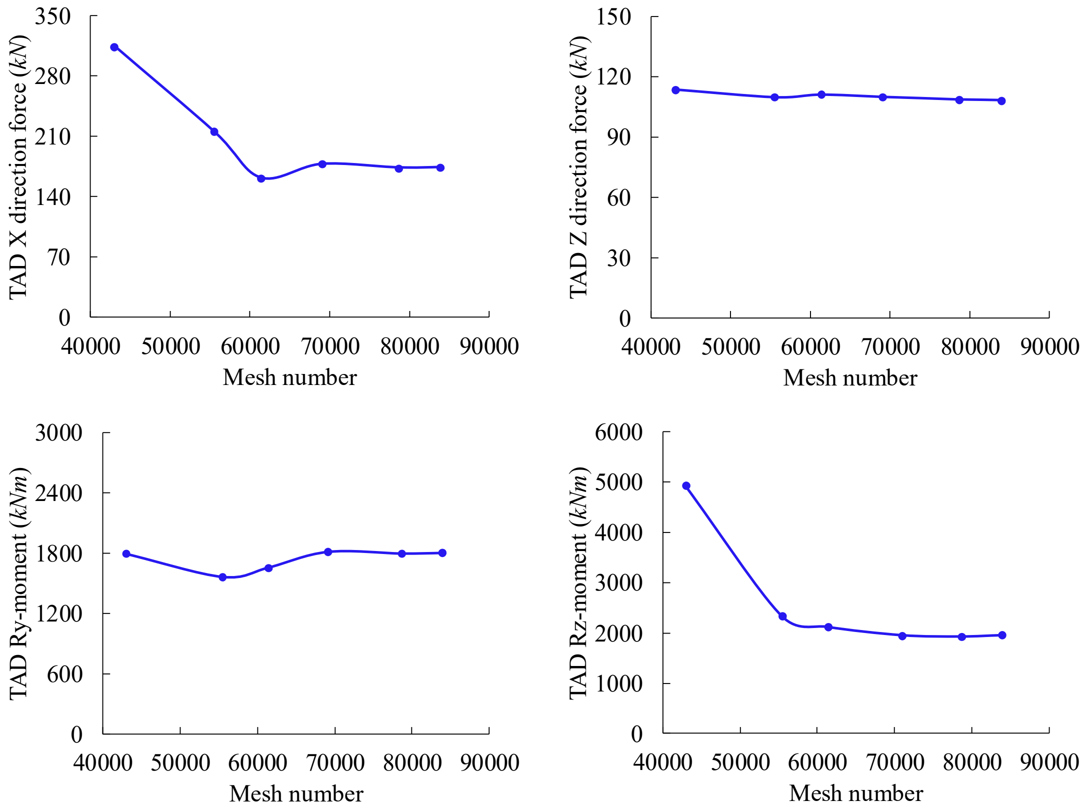

Fig 3 Second-order wave force on TLP and TAD in coupled model using different free surface meshes under 0° incident wave with frequency 1.2rad/s.

The result of the first-order wave load under different panel meshes of TLP and TAD are shown in Fig 2. It is noted that the results of first-order wave load become stable when the mesh size is smaller than 1.5m for both TLP with 6422 panels and TAD with 3988 panels indicating converged results of the first-order solutions.

According to Krisiansen et al. [36], the second-order results are very sensitive to the free surface mesh. Numerical calculations of the second-order wave load using different free surface meshes are carried out. The incident wave frequency equals 1.2 rad/s which means the double frequency for the second-order wave load is 2.4 rad/s as the highest incident frequency in this study. The results for the second-order wave load in surge, heave, pitch and yaw direction on both TLP and TAD are shown in Fig 3. As can be observed, most results of the second-order wave force become stable for the mesh number equaling or greater than 69004. Considering the results accuracy and computation time, the free surface mesh number with 78588 is selected for the simulations.

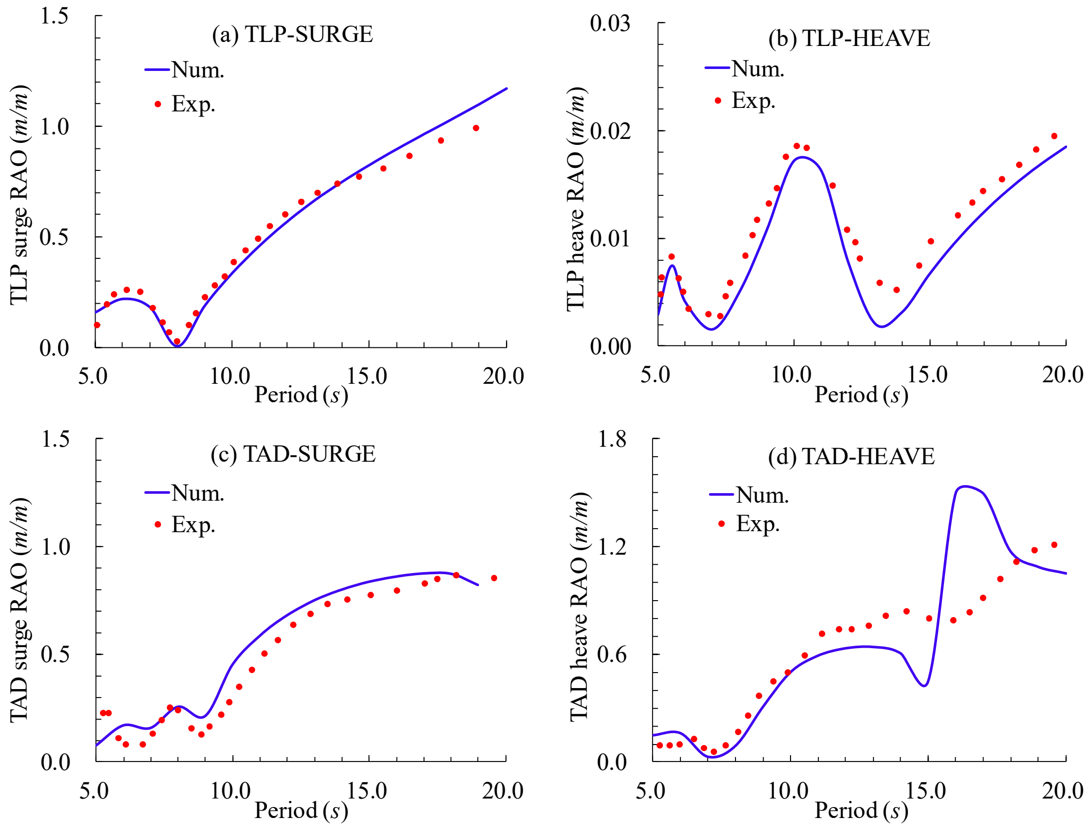

Fig 4 Surge and heave response of TLP isolated and TAD isolated model under 0° incident wave. (Numerical result Vs. Dong's [26] experiment result)

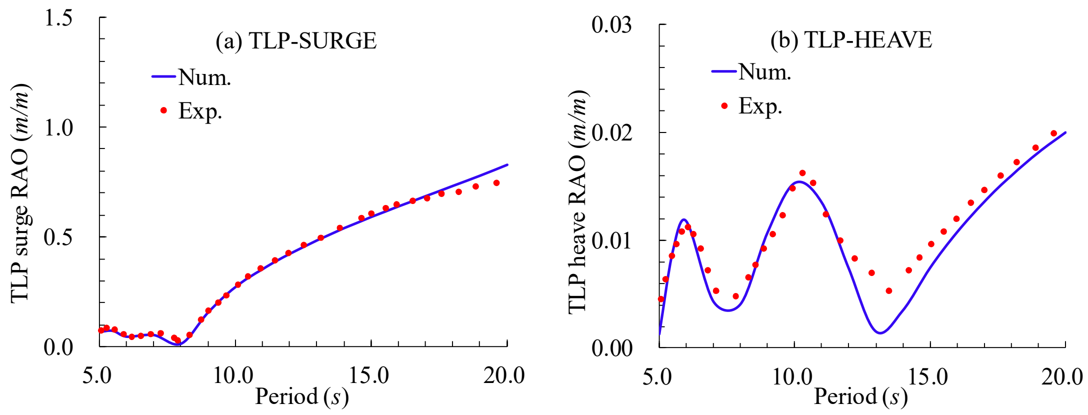

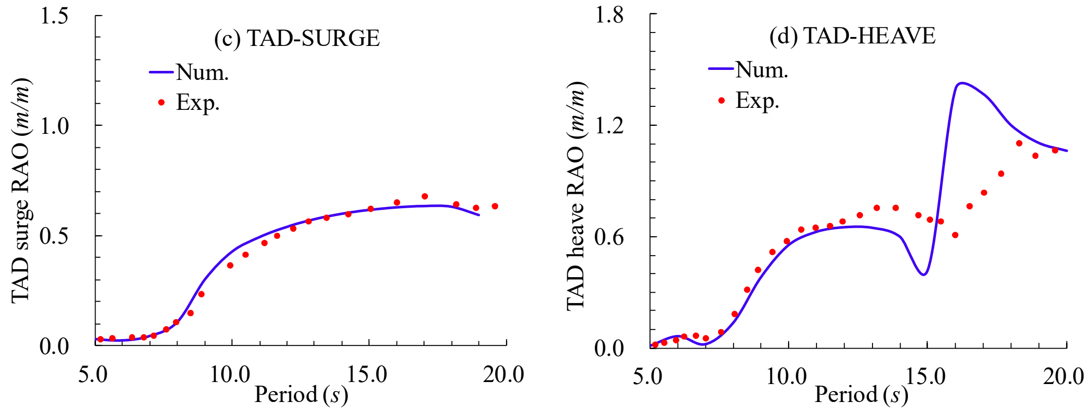

Fig 5 Surge and heave response of TLP isolated and TAD isolated model under 45° incident wave. (Numerical result Vs. Dong's [26] experiment result)

The global response of isolated TLP and isolated TAD model is shown in Fig 4 and Fig 5 (for both 0° and 45° wave heading as shown in Fig 1). Surge and heave motions are presented since they are more significant under 0° wave and 45° wave. The results show a good agreement in both surge and heave direction of TLP motion response, except that the differences occurring at the trough of heave motion. The discrepancy between the numerical and experiment result of heave motion is because of the restoring matrix used to replace the tendons and risers of TLP being over-simplification and ignoring some nonlinear characteristics of the mooring system. Additionally, the response of heave motion under 0° and 45° waves are practically the same. However, the surge motion under 45° is reduced significantly compared to that under 0°, for the wave load in that direction can be distributed into both surge and sway direction. The TAD surge motion response from the present numerical simulation has a good agreement with the model test (see Fig.5 (c)). The natural period of heave motion for TAD is observed in the numerical result at approximate 16.5s-17.5s. The main reason for the discrepancy between numerical predictions and experimental measurements is that the RAOs measured in experiment is conducted using white noise incident wave containing many wave period components rather than regular wave at each individual period. The motion response is difficult to achieve at the natural period under the white noise wave accurately. The heave motions under both 0° and 45° incident wave directions are approximately the same. However, similar to TLP, there is a significant reduction of surge motion under 45° incident wave compared to that under 0° incident wave.

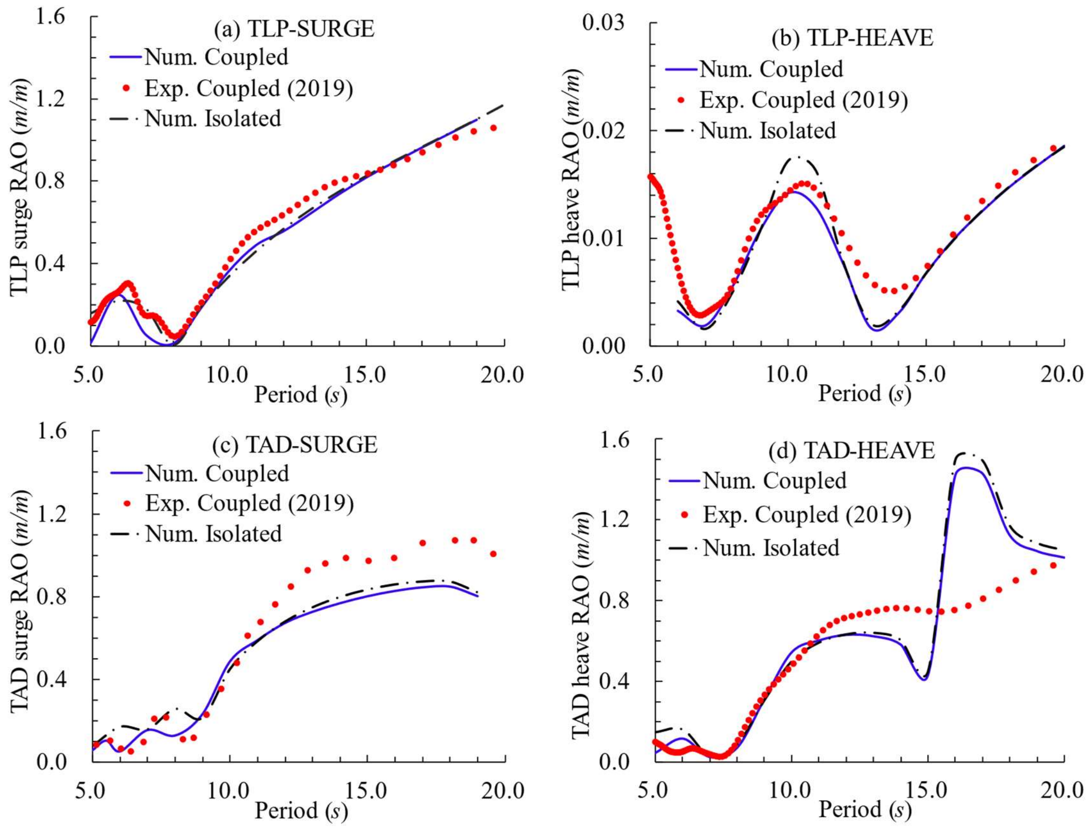

Fig 6 Surge and heave response of TLP and TAD in coupled system under 0°incident wave. (Numerical result Vs. Dong's [26] experiment result)

0° wave heading was selected for TLP-TAD coupled configuration to validate the multi-body coupled model. The global motion of coupled TLP-TAD model under 0° wave heading/EC1 is investigated and results are shown in Fig 6. The numerical results for isolated TLP and TAD are also shown in Fig 6 for comparison. Both horizontal and vertical motion RAOs are obtained. The discrepancy of TAD in surge motion (Fig.6 (c)) at large incident wave periods is observed. Since the incident irregular wave spectrum with T_s = 7s, there is very limited wave energy in the long wave period beyond 12s. However, the result at the shorter periods like 5s-6s shows a good agreement between the numerical and experimental results. The experimental result over the period around 12s is not as accurate as the shorter periods. A similar discrepancy is also reported by Dong et al. [26] for the comparison of results between the experiments and theoretical study.

There is a slight fluctuation appearing in the short periods in the surge of TAD (Fig.6 (c)) owing to the hydrodynamic interaction in the multi-body case. The surge motion of TLP in the multi-body system is approximately the same as TLP in isolation case. However, clear heave motion reduction for both TLP and TAD (Fig 6 (b) and (d)) is observed in TLP-TAD coupled system for a large range of wave period comparing with the isolated case. This is attributed to the connecting hawser between two platforms restricting the vertical motions of both TLP and TAD It is noted that the connecting hawsers are arranged in the horizontal plane at the beginning of simulation. However, considering the narrow spacing between the two platforms especially with the relative motion increasing between the two platforms in multi-body system, the restriction from the connecting hawsers to the vertical plane motions can be significantly increased. Under such condition, the hawser is clearly no longer in the horizontal plane and there will be a force component caused by hawser in vertical direction to restrict the vertical plane motions of the two platforms. Similar to the TLP/TAD in isolation model, there are differences in heave RAOs between model test and numerical result for TLP-TAD coupled model primarily due to the limitation of the incident wave energy. In general, the numerical and experimental results show a good agreement indicating that the numerical model is well established and thus will be employed in the following coupled analysis of the multi-body system.

The statistic results of relative motion measured by the distance between the coupled TLP-TAD connected by hawsers are shown in Table 3. It is noted that such relative motion or distance between the two adjacent platforms is dependent on the mechanical property of the hawsers and the hydrodynamic interaction between platforms. The results of relative motion for the coupled TLP-TAD shows good agreement.

Table 3 statistics of relative motion of TLP-TAD model with hydrodynamic interaction

Model	Maximum	Minimum	Range	Mean value	Standard Deviation	Discrepancy
Numerical	25.6m	23.9m	1.7m	24.75m	0.19	0.064
Experimental	23.9m	22.34m	1.64m	23.2m	0.21	

The acceleration of surge and heave for TLP and TAD in head wave (0°) are shown in Table 4 to validate the wave force on the TLP-TAD coupled model owing to the sensitivity of surge and heave for TLP and TAD respectively.

In Table 4, most statistic values of TLP and TAD acceleration show good agreement with the model test except the heave motion of TLP. The heave acceleration of TLP shows a large discrepancy of standard deviation. The discrepancy may be caused by the unusual mooring lines specifically including 8 tendons, 4 risers and 6 equivalent catenary lines of TLP. The arrangement of mooring system in the experiment is different to the numerical simulation, however, the total vertical force is kept same and the heave acceleration range of TLP between numerical and experiment result shows good agreement indicating the result in heave direction are reliable. The good agreement in the acceleration of TLP-TAD model and their relative motion demonstrates that the numerical simulations for both wave load and motion response of the TLP-TAD coupled system are reliable.

Table 4 The acceleration of TLP/TAD in numerical simulation and model test

Acceleration of TLP/TAD	Model	Maximum	Minimum	Range	Standard Deviation
Surge acceleration of TLP	Numerical	0.3677	-0.3925	0.7602	0.09518
	Experiment	0.392	-0.403	0.795	0.103
Heave acceleration of TLP	Numerical	0.1531	-0.1549	0.308	0.04868
	Experiment	0.147	-0.154	0.301	0.029
Surge acceleration of TAD	Numerical	0.285	-0.3026	0.588	0.073
	Experiment	0.32	-0.331	0.651	0.083
Heave acceleration of TAD	Numerical	0.1941	-0.1956	0.3897	0.056
	Experiment	0.192	-0.168	0.36	0.048

4.2 Wave load on multi-body configuration

4.2.1 First-order wave load on TLP and TAD in multi-body coupled model

The wave loads on TLP and TAD in both TLP-TAD coupled model and TLP/TAD isolated model with identical 0° incident wave (from negative *x*-direction shown in Fig 1) are shown in Fig 7 and Fig 8 respectively. The general trend of the first-order wave load in surge and heave directions on TLP and TAD for TLP-TAD coupled model and isolated model are similar. However, it can be clearly observed that there is a higher peak of wave load in surge direction on TLP at wave period around 6.5s (Fig 7 (a)). Since the TLP is at the upstream position (with 0° incident wave as shown in Fig 1), the only difference between isolated TLP and TLP-TAD coupled model is the existence of adjacent TAD downstream introducing the hydrodynamic interaction between two platforms. It indicates that the interaction between two platforms in coupled model is directly responsible to an increased amplitude of the first-order surge force on TLP at short wave period around 6.5s (Fig 7 (a)). The heave force on TLP (Fig 7 (b)) in coupled model shows a fluctuating pattern and increasing with rising period compared to a rather smooth increasing trend after an initial peak at low period for the TLP in isolation. This demonstrates that the interaction between two bodies of TLP-TAD coupled model leads to oscillatory heave force on TLP though it is positioned upstream (with 0° incident wave as shown in Fig 1) in addition to the increased first-order surge force on TLP. As shown in Fig 7 (a) and (b), with the increase of the incident wave period, the difference of the first-order wave loads between coupled model and isolated model becomes smaller indicating weakened interaction between TLP and TAD as the incident wave period increases.

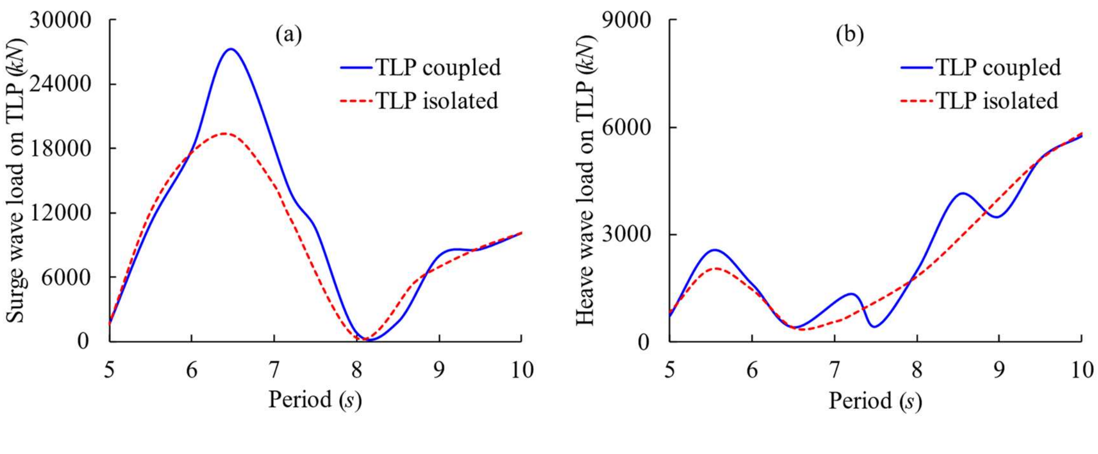

Fig 7. First-order wave load on TLP in (a) surge and (b) heave direction under 0° wave

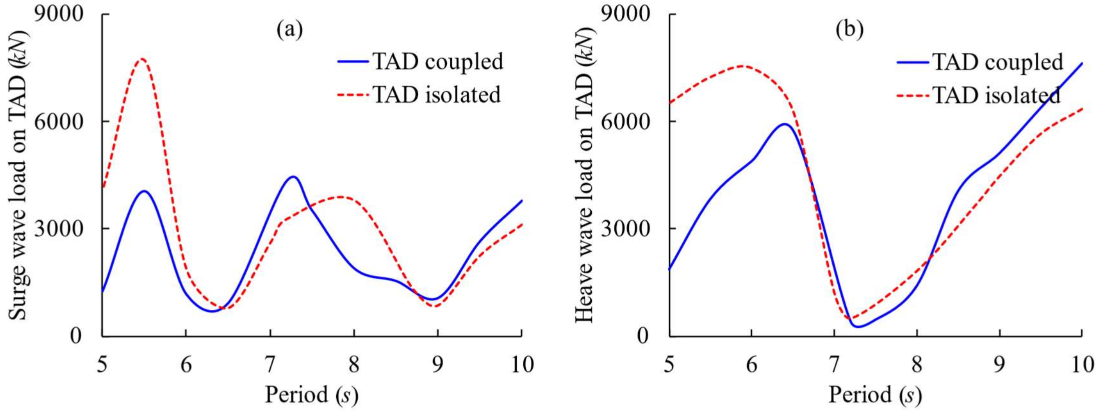

Fig 8. First-order wave load on TAD in (a) surge and (b) heave direction under 0° wave

The first-order wave force on TAD in surge and heave direction is shown in Fig 8. The shielding effect caused by the upstream TLP can reduce the wave load on TAD since it is located at the lee position of the configuration for the multi-body model. It can be clearly observed that the surge and heave wave load on TAD are reduced significantly by the adjacent TLP especially at the wave period around 5s-6.5s owing to the shielding effect. There is a large reduction of the incident wave energy caused by shielding effect leading the lower wave load on TAD. In addition, with weakened incident wave on the TAD, the interaction between bodies is also weakened. It is noted that the shielding effect becomes weak with increasing incident wave period because the ratio of the diameter of upstream structure (D) and incident wavelength (λ) becomes smaller. Consequently, the interaction between two platforms becomes stronger since less reduction of incident wave caused by shielding effect as incident wave period increase. Both shielding effect and hydrodynamic interaction between bodies have impacts on the wave load on TAD. As shown in Fig 8 (a) and (b), with the increasing wave period (6.5s-10s), the first-order wave loads on TAD in coupled model are sometimes larger than that in isolated model. This indicates that the shielding effect is not uniform across the incident wave period and additional factor due to the interaction between the two bodies in the coupled model may also contribute to the increase of wave load on TAD. It is noted that the influence of such interaction also exists in the shorter periods (5s-6.5s), though it is not dominated since the reduction of the incident wave caused by shielding effect. The shielding effect and interaction among the two adjacent bodies become weak with increasing incident wave period since the ratio of the diameter of upstream structure (D) and incident wavelength (λ) becomes smaller.

The wave force in coupled model sometimes becomes higher indicates that the shielding effect reduces more rapidly which makes the interaction between the two bodies more dominant resulting in higher wave force on TAD in coupled model.

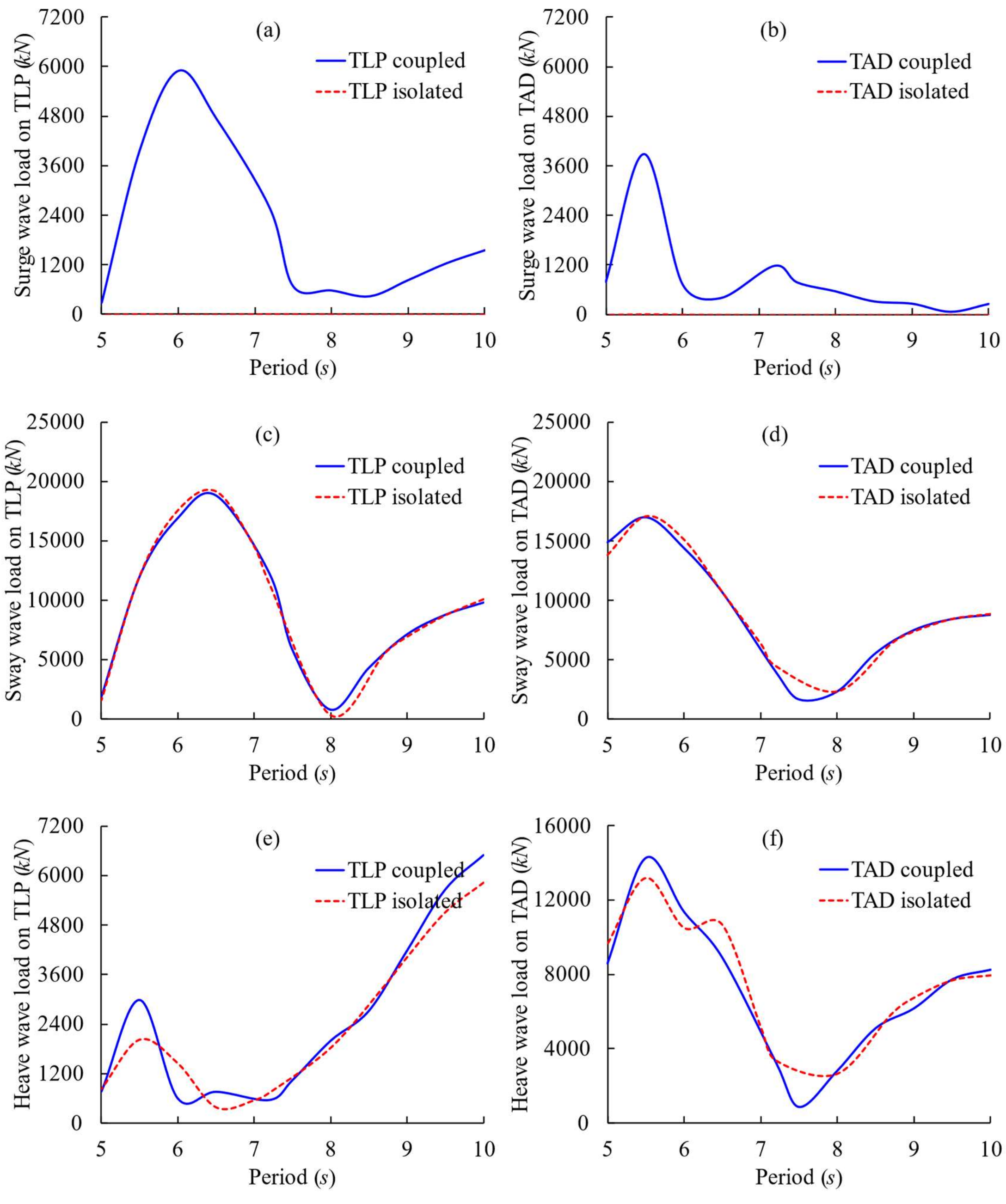

Fig 9 First-order wave load on TLP in (a) surge, (c) sway and (e) heave direction and TAD in (b) surge, (d) sway and (f) heave direction under 90° incident wave

To further examine the impact on wave loads due to interaction between adjacent platforms in multi-body system, a 90° incident wave which is from the negative Y-axis (beam sea condition) is selected to investigate the wave loads on TLP and TAD. There is no shielding effect on either

TLP or TAD under the beam sea. The first-order wave loads on TLP and TAD in surge, sway and heave are shown in Fig 9. The surge forces on TLP and TAD isolated model are seen very small comparing to those in the coupled model as shown in Fig 9 (a) and (b). In contrast to the isolated platform model, this indicates that interaction between two platforms in the coupled model introduces the first-order wave load in surge direction under beam sea condition. This is mainly due to the fact that the TLP and TAD in multi-body coupled model are arranged in surge direction. The surge components of diffraction and radiation caused by one body have impact on the other resulting in a much larger surge force on the TLP and TAD respectively in multi-body model. However, the first-order wave forces in sway direction on TLP and TAD in coupled model are similar to that in TLP/TAD isolated model. In addition, the first-order heave forces on TLP and TAD in coupled model and isolated model are similar indicating little impact of interaction between platforms on the first-order heave forces.

4.2.2 Second-order wave load on TLP and TAD in coupled model

The accurate estimate of sum-frequency wave force is crucial to the design of tendons preventing the undesired high-frequency “springing” and “ringing” of TLP in irregular wave. Such nonlinear effect can be further complicated by the interaction of the adjacent floating structures in the multi-body system. In the present study, the near-field integral method is applied to calculate the complete second-order quadric transfer function (QTF) matrix which is then used to calculate the sum-frequency wave load on TLP. When the incident irregular wave components’ periods are equal ($T_1 = T_2$), the sum-frequency wave load problem under irregular wave becomes identical to the double-frequency wave load problem in regular wave which is shown in the diagonal terms of the sum-frequency QTF matrix.

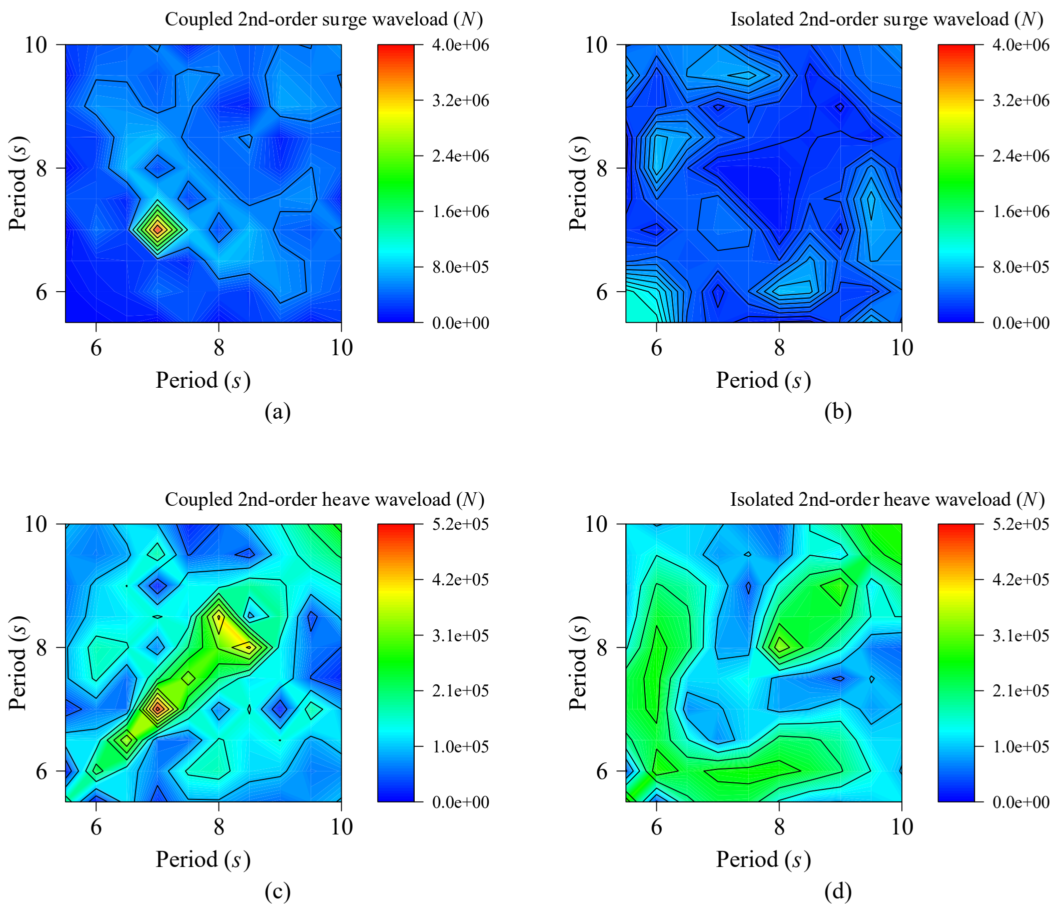

Fig. 10 Sum-frequency QTF matrix for wave loads on TLP under 0° incident wave. Surge force on TLP in: (a) TLP-TAD coupled model, and (b) TLP isolated model; Heave force on TLP in: (c) TLP-TAD coupled model, and (d) TLP isolated model.

The sum-frequency wave loads on TLP in coupled model in both surge and heave directions are compared with those in TLP in isolated model under 0° incident wave in Fig 10. Because of the existence of the adjacent TAD, the sum-frequency wave loads QTF has been altered. There is a peak value at $T_1 = T_2 = 7.1s$ of the TLP's surge sum-frequency QTF matrix in coupled model (Fig 10 (a)) comparing with the TLP in isolated model (Fig 10 (b)). It is noted that the peak of surge sum-frequency wave load in isolated TLP model occurs at the wave periods around $T_1 = T_2$=5.5s and it is lower than that in coupled model. When the incident wave components' periods $T_1 \neq T_2$, the sum-frequency surge force in coupled model is slightly higher than that in isolated model. The significant higher peak value at the diagonal line of the sum-frequency QTF matrix observed in coupled model (Fig 10 (a)) is caused by the existence of the TAD in coupled model. It means that the maximum double-frequency wave load on TLP becomes higher due to the interaction with the adjacent TAD. Similar to surge force, there is also an obvious peak when $T_1 = T_2$ in heave sum-frequency force QTF matrix (Fig 10 (c)). Most double-frequency wave loads in isolated model (Fig 10 (d)) are seen lower than those in coupled model (Fig 10 (c)) where a peak of wave load is observed in the diagonal line of the sum-frequency heave force QTF matrix. However, when the $T_1 \neq T_2$, the sum-frequency heave force on TLP in coupled model (Fig 10 (c)) is smaller than that in TLP in isolated model (Fig 10 (d)) especially at the area representing the combination of wave components frequencies $T_1 = 6$s to 9s and $T_2 = 6$s to 9s indicating that the interaction with the adjacent TAD can change the distribution of the sum-frequency wave force and increase the maximum value at double-frequency of the second-order wave force in heave direction. Such larger double-frequency wave force increase is the main characteristic that can lead to a highly nonlinear "ringing" response and fatigue damage to tendons and risers.

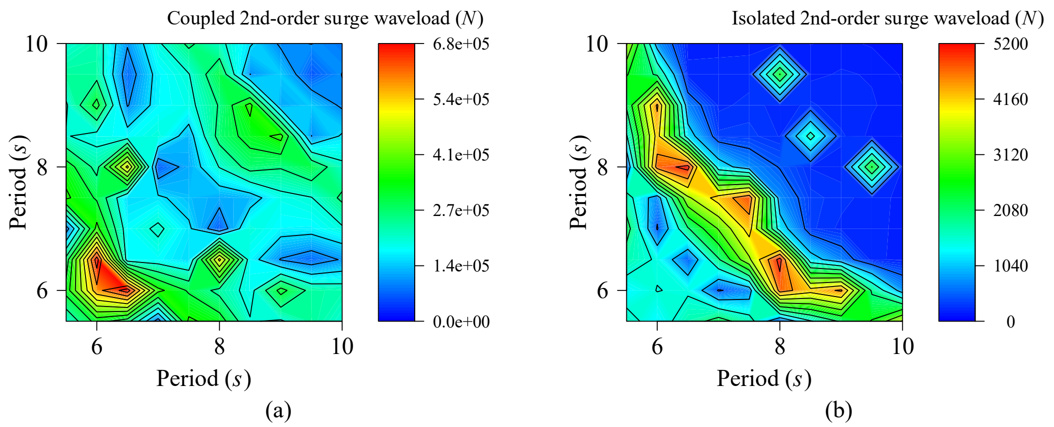

Fig 11 Sum-frequency QTF matrix of TLP under 90° incident wave. Surge wave load on TLP in (a) TLP-TAD coupled model, and (b) TLP isolated model.

Sum-frequency wave loads on TLP under beam sea (90° incident wave) are also investigated in the present study. Without shielding effect, the interaction between two bodies is the only factor influencing the wave loads on TLP and TAD in coupled model under the beam sea. It is noted that the legends of the second-order surge force in Fig 11 (a) and (b) are different since the interaction between TLP and TAD results in much higher sum-frequency wave load in surge direction on TLP in coupled model than that in the isolated model as shown in Fig 11 (a) and (b). However, the sum-frequency heave force on TLP in coupled model is lower than that in isolated model under the beam sea as shown in Fig 12 (a) and (b) owing to the interaction between TLP and TAD. According to Liu and Kim [37], the second-order heave force on isolated TLP is lower when the incident wave is not from the head direction since the dominated free surface force term is lower. It is noted that the total sum-frequency velocity potential used for calculation of TLP heave force in the coupled TLP-TAD model can be divided into three components, i.e., the incident wave potential, diffraction potential by TLP and the diffraction potential by TAD. The combined velocity potential is no longer in the direction which is vertical to the columns' arrangement direction of TLP due to the additional diffraction potential by TAD. Consequently, the adjacent TAD decreases the sum-frequency heave force on TLP by altering the total second-order sum-frequency velocity potential with additional diffraction potential by TAD.

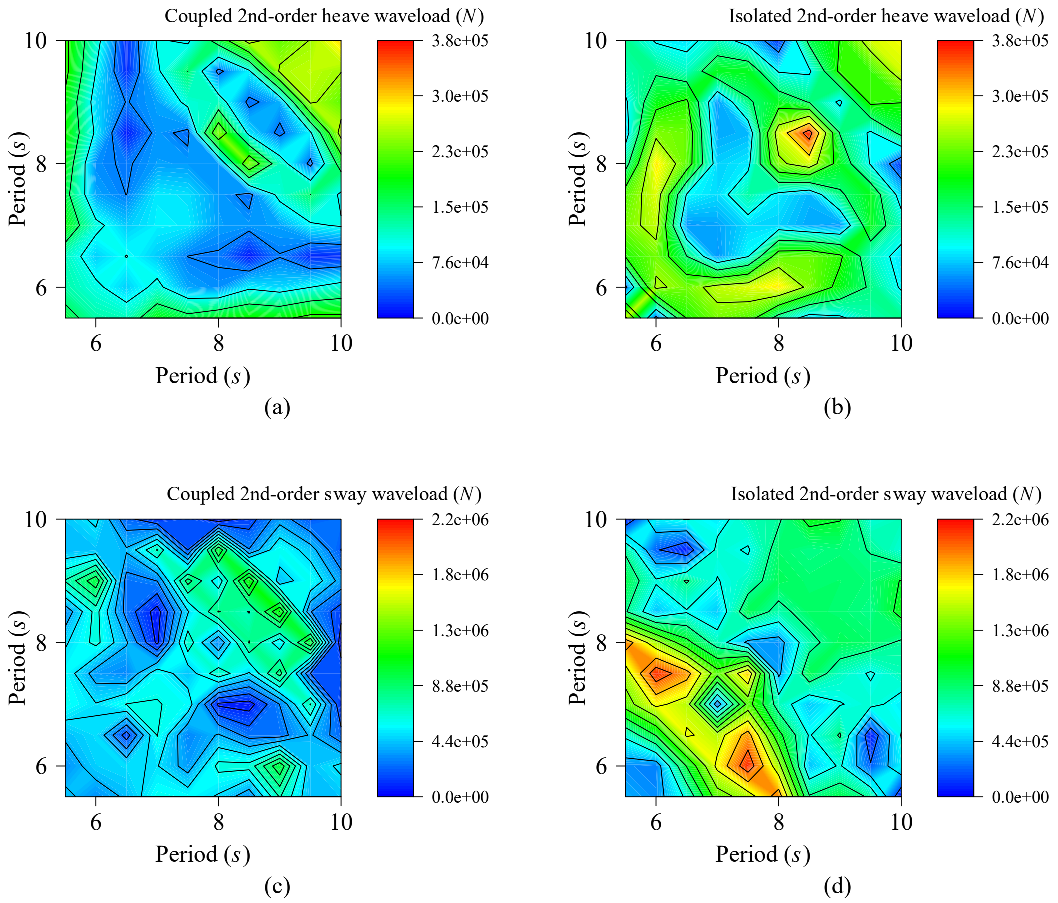

Fig 12 Sum-frequency QTF matrix of TLP under 90° incident wave. Heave wave load on TLP in (a) TLP-TAD coupled model, and (b) TLP isolated model. Sway wave load of TLP in (c): TLP-TAD coupled model and (d): TLP isolated model.

The prediction of low-frequency wave load on floating platform is very important especially for semi-submersible like TAD. Full difference-frequency QTF matrix can be calculated using near-field integral or mid-field integral method. Since it is very time consuming to calculate the full QTF matrix, Newman approximation is often applied in engineering design for the calculation of the wave drift load on TAD [38, 39].

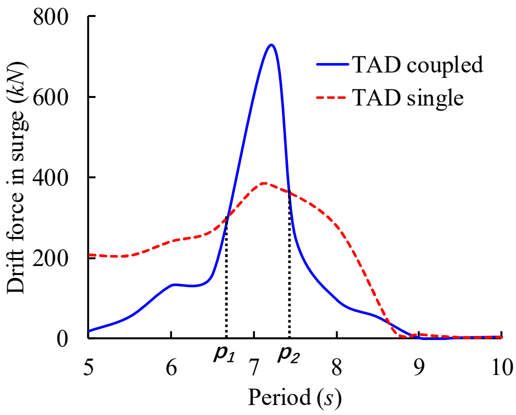

Fig 13 Surge difference-frequency drift force on TAD under 0°incident wave in TLP-TAD coupled model.

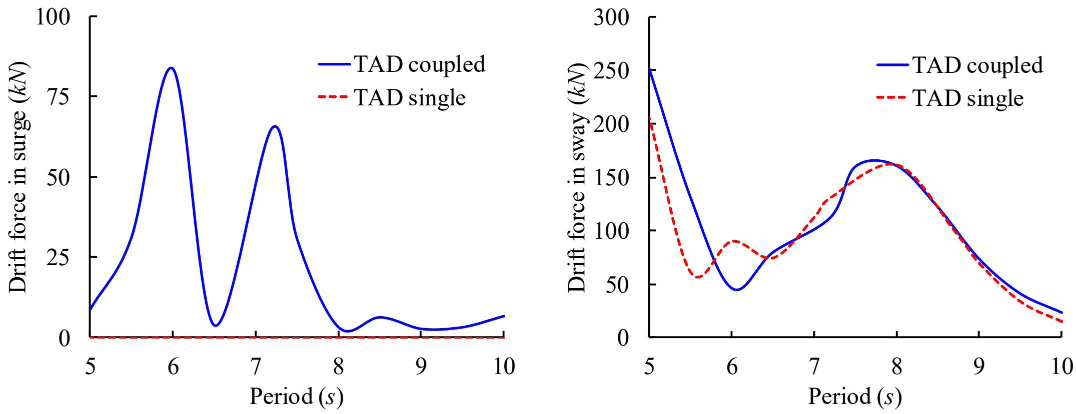

Fig 14 Difference-frequency drift force on TAD under 90°incident wave in TLP-TAD coupled model and TAD isolated model.

The surge wave drift load on TAD in TLP-TAD coupled model under 0° incident wave is shown in Fig 13. The wave load on TAD is influenced by the interaction between the two adjacent bodies and the shielding effect in coupled model. It is clearly seen in Fig 13 that, as the TAD is located at the lee position, the shielding effect makes the drift force on TAD in coupled model lower than that of TAD in isolation for a wide range of period. However, Fig. 13 also shows that the drift force on TAD is significantly higher in coupled model under the incident wave periods ranging between P1 to P2 and becomes lower after P2 indicating that the interaction between the two bodies amplifies the wave drift load on TAD. In fact, both shielding effect and interaction between TLP and TAD exist across the period range. Similar to the first-order surge force on TAD, the shielding effect is dominating when the wave period between 5s to P1 making the drift force on TAD in coupled model lower. However, the shielding effect decreases while the interaction increases with increasing wave period, and the competing effects on drift force on TAD in surge from the interaction and the shielding reach balance at P1, a crossing point, beyond that a rapid increase trend of drift force in coupled model and overtaking that of isolated model. It is a clear indication that interaction is dominating factor to the drift force over shielding effect between P1 and P2. The drift force on TAD in coupled model is seen a rapid decrease after reaching its peak until the second crossing point P2, followed by shielding effect becomes dominating influence over the interaction between the two platforms.

To further demonstrate that the impact of the interaction between two adjacent floating bodies on the drift force on TAD in coupled model, the beam sea condition is also selected in the investigation of wave drift load on TAD (Fig 14). Without shielding effect under 90° incident wave, Fig. 14 shows that the wave drift force on TAD in surge direction for the coupled model is much larger than that in isolated model. However, the wave drift load on TAD in sway direction for both coupled model and isolated model are similar. The impact of interaction on wave drift load is much more significant in surge direction owing to the arrangement of TLP and TAD in surge direction.

4.3 Wave load on TLP and TAD under irregular wave condition in time domain

Wave loads on TLP-TAD coupled model under EC1 and EC2 with 0° and 90° incident waves (heading sea and beam sea condition) are further analysed in time domain. The parameters of the incident irregular waves have been described in Section 2. The surge and heave forces on TLP in coupled model under EC1 are shown in Fig 15, which are obtained by performing the fast Fourier transform of corresponding wave load time series. The first-order surge force on TLP in coupled model is slightly higher than that of TLP in isolated model and the peak of sum-frequency wave force in surge direction on TLP in coupled model is nearly 3 times higher than the TLP in isolated model (Fig 15(a)). It indicates that the interaction between two platforms has impact on the surge wave load on TLP even it is in the upstream position of the configuration. The first-order heave forces are similar for both coupled model and isolated model (Fig 15(b)). The existence of the TAD does not appear to have a significant impact on the first-order heave force on TLP under the head sea condition and this is consistent with that demonstrated in Section 4.2.1 (see Fig. 7(b)). However, the sum-frequency heave forces on TLP in coupled model and TLP isolated model are different in Fig 15 (b). There is a peak point for the second-order force on TLP in coupled model at P1 in Fig 15(b). This can be further examined using QTF matrix shown in Fig 10 (c). There is a peak of the second-order heave force for sum-frequency QTF in Fig 10 (c) at the diagonal line representing the double-frequency wave load ($T_1 = T_2$ =7.1s) making the peak of sum-frequency heave force at $T =$ 3.57s shown in Fig 15 (b).

In isolated model, there is no obvious peak of the sum-frequency force in Fig 15 (b). It is worth noting that the sum-frequency heave force is mainly contributed by the sum-frequency effect while $T_1 \neq T_2$ especially when $T_1 =$ 6s to 9s and $T_2 =$ 6s to 9s as shown in sum-frequency QTF matrix (Fig 10 (d)). Since the sum-frequency heave force at the area representing the combination of wave components $T_1 =$ 6s to 9s and $T_2 =$ 6s to 9s are similar in QTF matrix, there is no significant peak of the sum-frequency heave force at the corresponding period from 3s to 4.5s in Fig 15 (b).

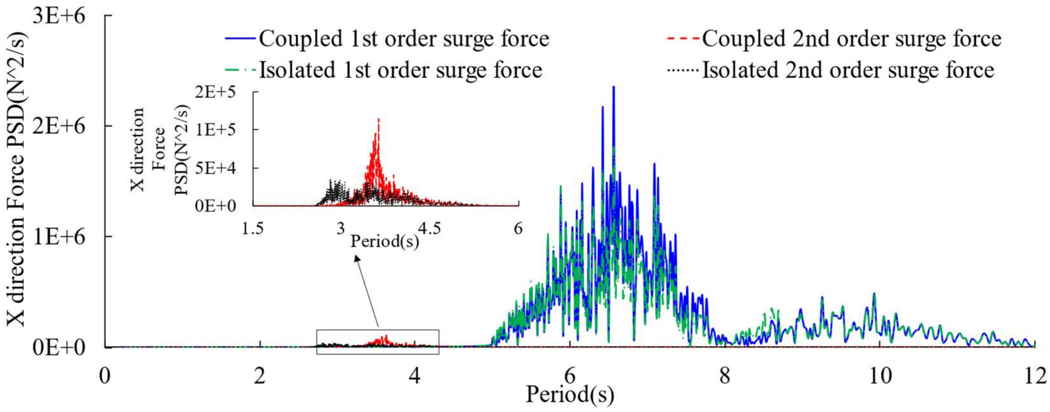

(a)

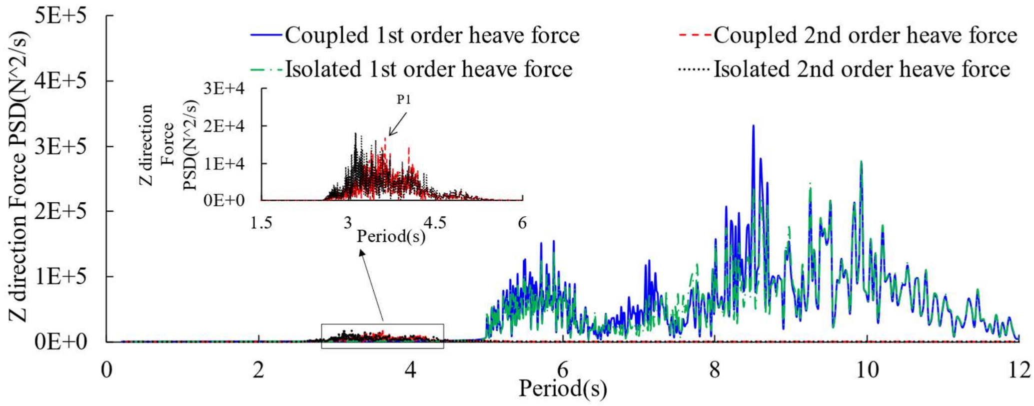

(b)

Fig 15 PSD (Power Spectral Density) of and the first-order and the second-order wave loads on TLP in coupled model and TLP isolated model under EC1: (a) surge; (b) heave.

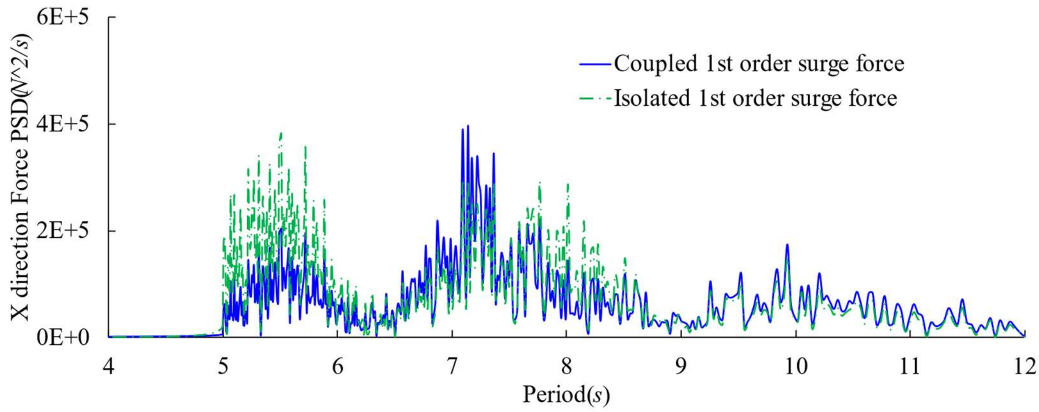

(a)

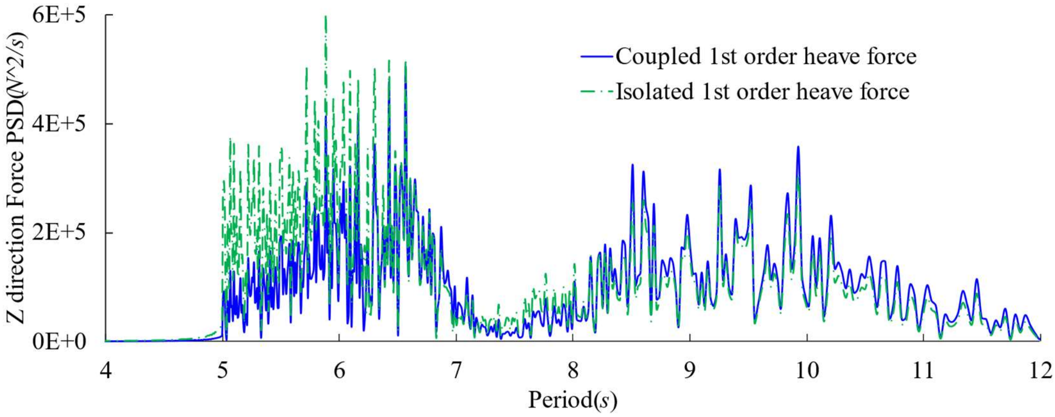

(b)

Fig 16 PSD (Power Spectral Density) of wave load on TAD in coupled model and TAD isolated model under EC1: (a) surge; (b) heave.

Similar to TLP in TLP-TAD coupled model, the first-order wave force on TAD under EC1 in surge and heave direction are also calculated and shown in Fig 16 (a) and (b) respectively. The wave forces on these two directions in isolated model appear to be approximately 87% in surge and 32% in heave higher than those in coupled model for the period between 5s-6.5s. However, the first-order wave force (both surge force in Fig 16 (a) and heave force in Fig 16 (b)) in coupled model and isolated model become similar with the increasing period (T>7s). These first-order wave forces calculated in time domain under the irregular wave condition also validate the characteristics of the wave load on TAD shown in Fig 8.

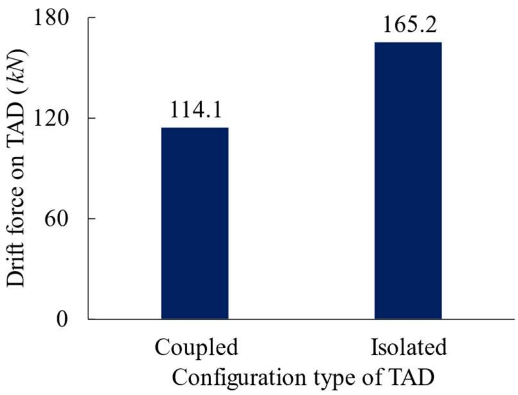

Fig 17 The mean value of the wave drift load (surge) on TAD in coupled model and TAD isolated model under 0° incident wave condition.

Fig 17 shows that the mean value of drift force in surge direction on TAD in coupled model is lower than that in TAD in isolated model under the 0° irregular wave. For a wave spectrum with energy distribution of the incident wave around 5-10s under EC1, there are many wave components considered at different periods in Fig 17. The mean value of the surge drift force on TAD in coupled model under EC1 is lower indicating that shielding effect is still dominating under the irregular wave condition with consideration of all incident wave components.

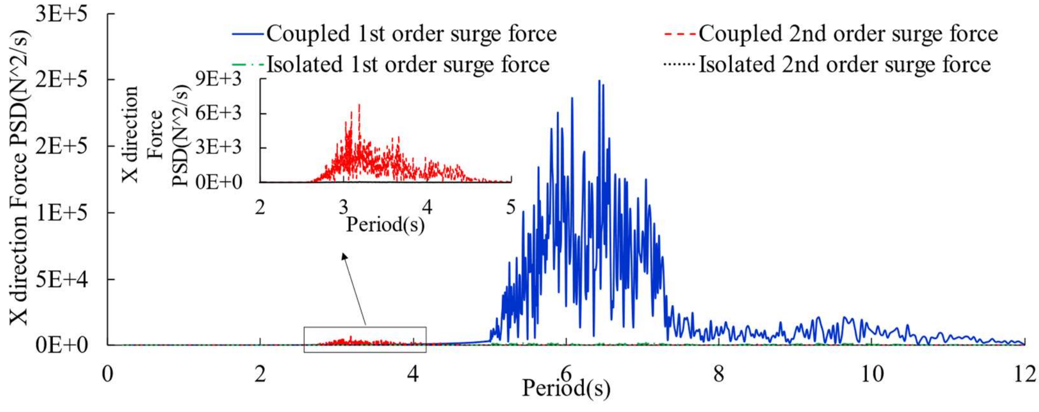

Fig 18 PSD (Power Spectral Density) of surge wave load on TLP in coupled model and TLP isolated model under beam sea.

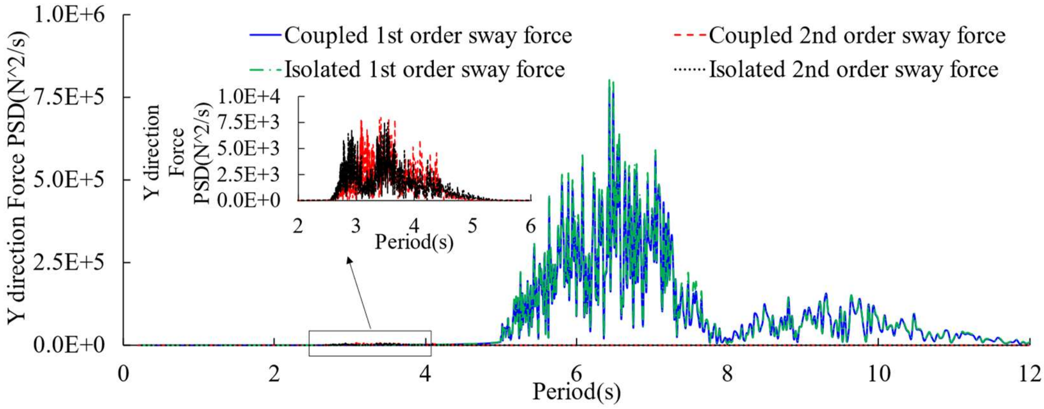

(a)

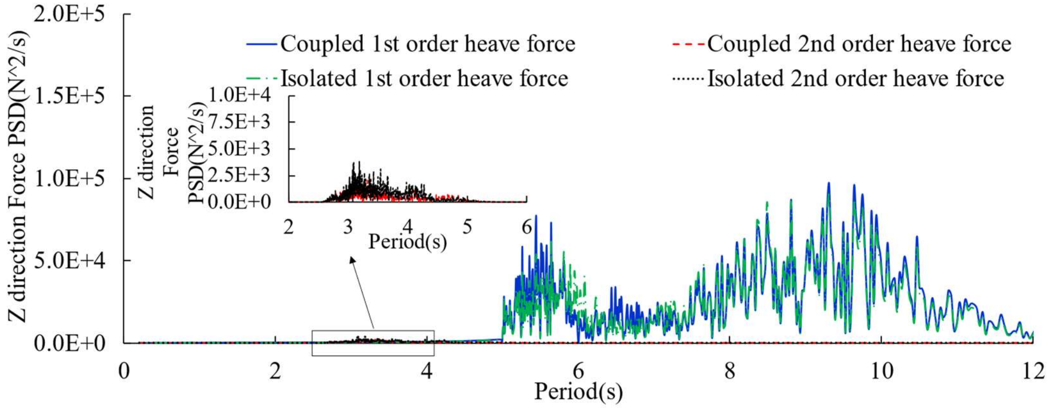

(b)

Fig 19 PSD (Power Spectral Density) of sway (a) and heave (b) wave load on TLP in coupled model and TLP isolated model under beam sea.

The surge forces on TLP in both coupled and isolated model under the beam sea are shown in Fig 18. The sum-frequency and wave frequency surge loads on TLP in isolated model are significantly lower than those in the coupled model which are consistent with the features observed in Fig 9 and Fig 11. The first-order wave force and sum-frequency wave force on TLP in sway and heave direction are shown in Fig 19. There is no significant difference between the first-order wave forces on TLP in coupled model and the isolated model. However, the sum-frequency wave forces on TLP in sway show different distribution with increasing wave period in coupled model and the isolated model. The peak value of heave force due to sum-frequency in isolated model is about 45% higher than that in coupled model which is also observed in Fig11 (c) and (d).

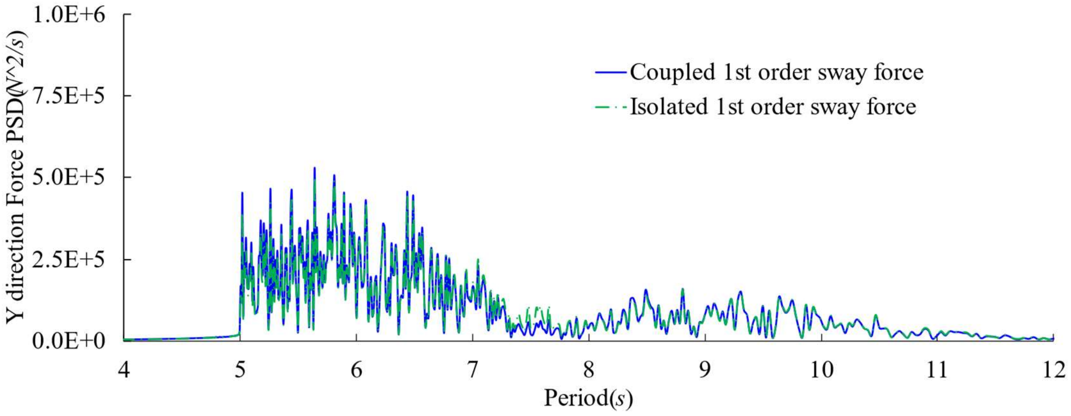

(a)

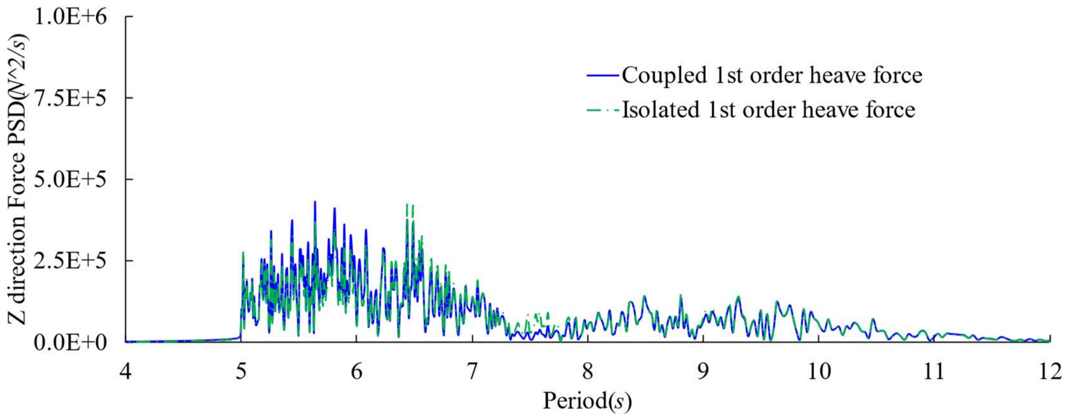

(b)

Fig 20 PSD (Power Spectral Density) of sway (a) and heave (b) wave load on TAD in coupled model and TAD isolated model under beam sea.

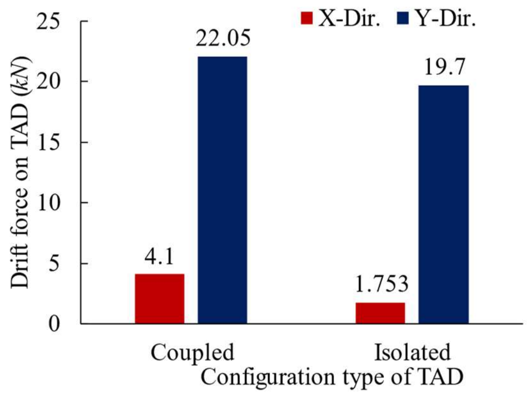

Fig 21 The mean value of the wave drift load in X-direction (surge) and Y-direction (sway) on TAD in coupled model and TAD isolated model under the beam sea.

The sway and heave wave frequency forces on TAD in multi-body coupled model and isolated model under the beam sea condition are shown in Fig 20. The wave frequency loads on TAD in both models are similar which is further validation to the features observed in Fig 9 (d) and (f) indicating that the interaction between two floating bodies in coupled model has little impact on the first-order wave force in sway and heave direction. The mean value of the wave drift loads in surge and sway direction under the beam sea condition are shown in Fig 21 without shielding effect between the two bodies. The mean value of the wave drift load on TAD in sway direction is slightly higher (10.6%) in coupled model while the surge drift force in coupled model is more than twice that in the isolated model. This indicates the interaction between two adjacent floating bodies in coupled model can increase the wave drift load in surge direction owing to the bodies are arranged in surge direction. This characteristic of wave forces in platforms arrangement in coupled model should be considered in the prediction of relative motion and practical design of the gangway between platforms.

Conclusions

The multi-body coupled TLP-TAD system under 0° and 90° incident waves are investigated based on numerical simulation. The numerical model is rigorously validated with the experiment results. The global motion responses of the multi-body system and the wave forces on platforms are examined in detail. Both frequency and time domain approaches are adopted in numerical simulations to consider the effect of hydrodynamic interaction between two bodies and nonlinear effects. Based on the present research, the main conclusions are as follow:

1. The interaction between two adjacent floating bodies increases both the first-order and the second-order wave force on the two bodies along their arrangement direction in multi-body system. For the structure at the lee position, both shielding effect and the interaction between the two bodies have great impacts on the wave force. This should be taken into the consideration in the prediction of the relative motion and design of the gangway between platforms.
2. Under the beam sea condition, the wave loads in surge direction (which is transverse to the

incident wave) on TLP/TAD in coupled model cannot be neglected since the diffraction and radiation in surge direction caused by adjacent platform. This should be a concern in the gangway design between two platforms.

3. The influence of interaction between the two bodies on TLP's sum-frequency heave force in multi-body system highly depends on the wave direction. The peak value of sum-frequency QTF matrix in heave in coupled model under heading wave is much higher than that of TLP in isolated model. The sum-frequency QTF matrix in heave in coupled model under the beam sea is lower than that of TLP in isolated model. This characteristic of sum-frequency force in heave is a crucial design feature to avoid the significant nonlinear (high frequency "springing" and "ringing") wave load which often induces TLP undergoing resonant motion in vertical planes and further leads to fatigue load to tendons and risers in TLP-TAD coupled model.
4. The drift force on TAD in surge is increased by the interaction between the two floating bodies. Meanwhile, the shielding effect is also existing across periods in head sea conditions. The combination of these two effects may lead the drift force on TAD much higher in some range of wave period and leads the top tension of mooring lines of TAD to increase suddenly.

References

[1] R. Kota, K. Yip, S.A. Jamal, Design and Installation of Coupled Mooring System for Tender-Assisted Drilling at a Deepwater TLP, in: Offshore Technology Conference Asia, Offshore Technology Conference, 2018.

[2] R. Kota, S. Amurol, H. Tan–Sabah, Design and Operation of Coupled Mooring System for Tender-Assisted Drilling at Malikai TLP, in: Offshore Technology Conference, Offshore Technology Conference, 2018.

[3] E. Smith, W. Dixon, Tender-supported operations at the Odin field, Journal of petroleum technology, 39 (1987) 324-330.

[4] E. Adrian, S. Wong, Overview of the Malikai Project, in: Offshore Technology Conference, Offshore Technology Conference, 2018.

[5] C.H. Kim, The hydrodynamic interaction between two cylindrical bodies floating in beam seas, in, 1972.
[6] A.E. Loken, Hydrodynamic interaction between several floating bodies of arbitray form in waves, in: International Symposium on Hydrodynamics in Ocean Engineering, The Norwegian Institute of Technology, 1981.
[7] W. Lu, W. Zhao, P. Taylor, J. Yang, L. Xiao, X. Li, Linearity and nonlinearity in wave run-up and air-gap response for a semi-submersible platform under irregular wave excitation, Applied Ocean Research, 104 (2020) 102218.
[8] F. Jean-Robert, M. Naciri, C. Xiao-Bo, Hydrodynamics of two side-by-side vessels experiments and numerical simulations, in: The Sixteenth International Offshore and Polar Engineering Conference, International Society of Offshore and Polar Engineers, 2006.
[9] R. Watai, P. Dinoi, F. Ruggeri, A. Souto-Iglesias, A. Simos, Rankine time-domain method with application to side-by-side gap flow modeling, Applied Ocean Research, 50 (2015) 69-90.
[10] W. Zhao, J. Yang, Z. Hu, L. Tao, Prediction of hydrodynamic performance of an FLNG system in side-by-side offloading operation, Journal of Fluids and Structures, 46 (2014) 89-110.
[11] M. Perić, C. Swan, An experimental study of the wave excitation in the gap between two closely spaced bodies, with implications for LNG offloading, Applied Ocean Research, 51 (2015) 320-330.
[12] Y. Jin, S. Chai, J. Duffy, C. Chin, N. Bose, Hydrodynamics of a conceptual FLNG system in side-by-side offloading operation, Ships and Offshore Structures, 14 (2019) 104-124.
[13] S. Ganesan, D. Sen, Time domain simulation of side-by-side floating bodies using a 3D numerical wave tank approach, Applied Ocean Research, 58 (2016) 189-217.
[14] W. Zhao, P. Taylor, H. Wolgamot, B. Molin, R.E. Taylor, Group dynamics and wave resonances in a narrow gap: modes and reduced group velocity, Journal of Fluid Mechanics, 883 (2020).
[15] W. Huang, B. Li, X. Chen, R. Araujo, Numerical and experimental studies on dynamic gangway response between monohull flotel and FPSO in non-parallel side-by-side configuration, Ocean Engineering, 149 (2018) 341-357.
[16] H. Ok, S. Lee, J. Choi, Numerical simulation of motion of single and side-by-side vessels in regular waves using OpenFOAM, Ships and Offshore Structures, 12 (2017) 793-803.

[17] M. Wu, Numerical analysis of docking operation between service vessels and offshore wind turbines, Ocean engineering, 91 (2014) 379-388.

[18] X. Xu, J.-m. Yang, X. Li, L.-y. Xu, Time-domain simulation for coupled motions of three barges moored side-by-side in floatover operation, China ocean engineering, 29 (2015) 155-168.

[19] J. Xia, R. Taghipour, Feasibility of TLP with Tender Assisted Drilling for Northwest Australian Waters-A Case Study, in: Offshore Technology Conference, Offshore Technology Conference, 2012.

[20] Y.-M. Choi, B.W. Nam, S.Y. Hong, D.W. Jung, H.J. Kim, Coupled motion analysis of a tension leg platform with a tender semi-submersible system, Ocean Engineering, 156 (2018) 224-239.

[21] L. Sun, R.E. Taylor, Y.S. Choo, Multi-body dynamic analysis of float-over installations, Ocean engineering, 51 (2012) 1-15.

[22] M.A. Ramirez, A.C. Fernandes, Coupled wave motions on a tension leg platform and tender-assisted drilling, Marine Systems & Ocean Technology, 12 (2017) 150-165.

[23] Y. Liang, L. Tao, Hydrodynamics interactions on vortex-induced motions of a multi-body floating system, in: International Conference on Offshore Mechanics and Arctic Engineering, American Society of Mechanical Engineers, 2019, pp. V009T013A037.

[24] H. Abyn, A. Maimun, J. Jaswar, M. Rafiqul Islam, C. Siow, B. Bodaghi, TLP Motion Effect on Semisubmersible Motion, in: Offshore Technology Conference-Asia, Offshore Technology Conference, 2014.

[25] A. Maimun, Z.R. Ismail, M.M. Tofa, H. Abyn, Hydrodynamic Interaction Between Tension Leg Platform (TLP) and Semisubmersible in Close Proximity, in: Offshore Technology Conference Asia, Offshore Technology Conference, 2016.

[26] Q. Dong, H. Lu, J. Yang, X. Guo, Dynamic gangway responses between TLP and semi-submersible platform during tender-assisted drilling, Marine Structures, 67 (2019) 102645.

[27] M.-H. Kim, D.K. Yue, The complete second-order diffraction solution for an axisymmetric body Part 1. Monochromatic incident waves, Journal of Fluid Mechanics, 200 (1989) 235-264.

[28] M.-H. Kim, D.K. Yue, The complete second-order diffraction solution for an axisymmetric body Part 2. Bichromatic incident waves and body motions, Journal of Fluid Mechanics, 211 (1990) 557-593.

[29] C. Wang, G. Wu, Time domain analysis of second-order wave diffraction by an array of vertical cylinders, Journal of Fluids and Structures, 23 (2007) 605-631.

[30] P. McIver, Mean drift forces on arrays of bodies due to incident long waves, Brunel University Mathematics Technical Papers collection;, (1986).

[31] C.-H. Lee, WAMIT THEORY MANUAL, (1995).

[32] B. Li, W. Huang, X. Chen, A numerical study of dynamic response of crane semi-submersible along TLP in tender-assisted drilling operation, Ships and Offshore Structures, 13 (2018) 273-286.

[33] DNV, SIMA USER MANUAL, (2019).

[34] H. Wei, L. Xiao, X. Tian, Y. Kou, Four-level screening method for multi-variable truncation design of deepwater mooring system, Marine Structures, 51 (2017) 40-64.

[35] W. Biao, Y. Xiaolong, Q. Licheng, W. Lei, A comparative study on model test and numerical analysis of wave basin based on tension leg platform in south china sea, Research and Exploration in Laboratory, 37 (2018) 53-57.

[36] T. Kristiansen, R. Baarholm, C.T. Stansberg, Validation of second-order analysis in predicting diffracted wave elevation around a vertical circular cylinder, in: The Fourteenth International Offshore and Polar Engineering Conference, International Society of Offshore and Polar Engineers, 2004.

[37] Y. Liu, M. Kim, C. Kim, The Computation of Second-Order Mean and Double-Frequency Wave Loads on a Compliant TLP by HODEM, International Journal of Offshore and Polar Engineering, 5 (1995).

[38] J.N. Newman, Second-order, slowly-varying forces on vessels in irregular waves, (1974).

[39] J.N. Newman, Algorithms for the free-surface Green function, Journal of engineering mathematics, 19 (1985) 57-67.